



# Influence of Bi substitution on structural and optical properties of LaFeO<sub>3</sub> perovskite

Mohammed Sadok MAHBOUB<sup>1,\*</sup>, Ouarda BEN ALI<sup>1</sup>, Soria ZEROUAL<sup>1</sup>, Ghani RIHIA<sup>1</sup>, Mourad MIMOUNI<sup>1</sup>, Imad HAMADNEH<sup>2</sup>, Samir BAYOU<sup>3</sup>, Hani BOULAHBEL<sup>4</sup>, Adel BENARFA<sup>5</sup>, and Ferhat REHOUMA<sup>1</sup>

<sup>1</sup> LEVRES Laboratory, University of El Oued, 39000 El Oued, Algeria

<sup>2</sup> Department of Chemistry, Faculty of Science, University of Jordan, Amman 11942, Jordan

<sup>3</sup> Chemistry department, Faculty of Exact Sciences, University of El Oued, 39000 El Oued, Algeria

<sup>4</sup> Centre de Recherche Scientifique et Technique en Analyses Physico-Chimiques BP 384, Siège ex-Pasna Zone Industrielle Bou-Ismaïl, CP 42004 Tipaza, Algeria

<sup>5</sup> Centre de Recherche Scientifique Et Technique en Analyses Physico-Chimiques (CRAPC)-PTAPC, P.O. Box 0354, Laghouat 03000, Algeria

\*Corresponding author e-mail: mahboub-mohammedsadok@univ-eloued.dz

## Received date:

11 September 2023

## Revised date:

28 May 2024

## Accepted date:

11 September 2024

## Keywords:

Band gap energy;

Nanoparticle;

Photocatalytic;

Sol-gel;

Solar cell

## Abstract

The sol-gel self-ignition method has successfully synthesized a series of homogenous perovskites La<sub>1-x</sub>Bi<sub>x</sub>FeO<sub>3</sub> (x=0.0, 0.2, 0.4, 0.6, and 0.8) nanoparticles. Rietveld refinement results from XRD patterns revealed no secondary phases in pure and Bi-substituted LaFeO<sub>3</sub> samples. The structural transition from orthorhombic at x = 0.0 until x=0.6 (space group Pbnm) to rhombohedral at x=0.8 (space group R3c) was observed. Lattice parameter values increase slightly with Bi concentration due to the substitution of Bi in the LaFeO<sub>3</sub> structure. The average crystallite size D was found to vary between 19 nm and 50 nm. The combination of XRD and SEM demonstrated that the prepared Bi-doped LaFeO<sub>3</sub> is a single-phase perovskite with a relatively homogeneous particle size distribution. SEM images revealed quasi-spherical particle shapes. FTIR spectra identify the metal oxide bending vibrations at about 536 cm<sup>-1</sup> and 717 cm<sup>-1</sup> attributed to Fe-O and La-O bonds, respectively. No significant effect of Bi substitution from 0% up to 60% on crystal volume was observed, as confirmed by FTIR spectroscopy, which showed no shift in La/Fe-O bending vibration modes with increasing Bi content. The obtained results indicated that the E<sub>g</sub> values exhibited a monotone decrease with an increase in Bi ratio. The band gap values varied from 2.2 eV for pure LaFeO<sub>3</sub> to 1.85, 1.76, 1.54 and 1.35 eV for the substitutions of 20%, 40%, 60% and 80% respectively. Hence, the sample La<sub>0.2</sub>Bi<sub>0.8</sub>FeO<sub>3</sub> with the small band gap value can be used as a promising candidate in solar cell applications.

## 1. Introduction

Recently, there has been a surge in interest in the preparation of complex perovskite oxides due to their attractive physical and chemical properties. Prominent among these materials are perovskite lanthanum ferrite and related compounds, defined by the general formula La<sub>1-x</sub>A<sub>x</sub>FeO<sub>3</sub> (A = Ca, Ce, Sr, Sm, or other rare earth elements). These compounds are garnering attention due to their wide-ranging applications in fuel cell technology [1,2], catalysis [3,4], sensor material for the detection of humidity and alcohol [5,6], environmental monitoring systems [7], water splitting [8,9] and photocatalysis [10].

The semiconductor photocatalytic technique has gained marvelous attention in recent years, attributed to its cost-effectiveness, non-toxicity, high chemical and thermal stability, and environmentally friendly nature [11-13]. LaFeO<sub>3</sub> NPs, with a narrow band gap of about 2.0 eV to 2.6 eV, have been employed as a visible-light-driven catalyst; however, their photocatalytic efficiency is limited.

Peters and Buonassisi [14] conducted a comprehensive study on solar cells with various band-gaps, including established technologies like Si and CdTe, as well as emerging materials such as perovskites. Their investigation revealed that the band-gap for which the highest

efficiency is achieved varies very little, with an optimum value of 1.35 ± 0.01 eV. Additionally, nanocomposites of mesoscopic TiO<sub>2</sub> modified with nanoparticles of the inorganic perovskite LaFeO<sub>3</sub>, denoted as LaFeO<sub>3</sub>:TiO<sub>2</sub>, have been developed. These nanocomposites serve as electron transport layers (ETLs) in perovskite solar cells (PCSs), contributing significantly to the utilization of renewable energy [15].

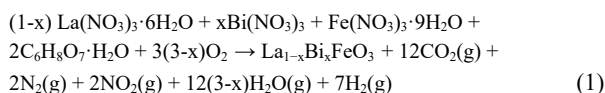
Doping LaFeO<sub>3</sub> NPs with non-precious metals, such as La<sub>1-x</sub>Sb<sub>x</sub>FeO<sub>3</sub> [16] and La<sub>1-y</sub>Sr<sub>y</sub>Ni<sub>1-x</sub>Fe<sub>x</sub>O<sub>3</sub> [17], has demonstrated enhanced photocatalytic activity. Moreover, modification of LaFeO<sub>3</sub> via chemical substitution with divalent cations has also been widely studied, and changes in its physical properties and performance characteristics have been reported [18-25]. For instance, Cu substitution in (La, Sr) FeO<sub>3</sub> reduces unit cell volume and provides moderate absorbance of visible light, making it suitable for photocatalytic applications at low temperatures [20]. On another hand, Fitria *et al.* [26] revealed that La<sub>1-x</sub>Bi<sub>x</sub>FeO<sub>3</sub> (x = 0.1, 0.3, and 0.5) samples exhibited the single phase orthorhombic structure with Pnma space group, and increasing Bi content led to a decrease in the dielectric constant. Likewise, Yao *et al.* [27] reported that the partial substitution of La atoms by Bi (0.0 ≤ x ≤ 0.5) results in single-phase compounds crystallized into an orthorhombic crystal structure (space group Pnma). Conversely, Wanjun *et al.* [28]

suggested that the addition of more Bi-doping in  $\text{La}_{1-x}\text{Bi}_x\text{FeO}_3$  powders ( $0 \leq x \leq 0.2$ ) may transform the orthorhombic Pbnm structure into the rhombohedral R3c structure gradually. In another study, Ahmed *et al.* [29] observed traces of a secondary phase with a rhombohedral structure.

Despite these studies, there is still a gap in systematic and comparative analysis regarding the effect of Bi-substituted La-site on the structural and optical properties of  $\text{LaFeO}_3$ . Therefore, this study aims to address this gap by investigating the structural, morphological, and optical aspects of a series of  $\text{La}_{1-x}\text{Bi}_x\text{FeO}_3$  ( $x=0.0, 0.2, 0.4, 0.6,$  and  $0.8$ ) were investigated using X-Ray powder diffraction (XRPD), SEM/EDX, FTIR, and UV-Visible spectroscopy.

## 2. Experimental

The solution-gelation self-ignition technique was used to prepare Bismuth-doped Lanthanum ferrite ( $\text{La}_{1-x}\text{Bi}_x\text{FeO}_3$ ). Stoichiometric amounts of Lanthanum nitrate ( $\text{La}(\text{NO}_3)_3 \cdot 6\text{H}_2\text{O}$ , Sigma-Aldrich,  $\geq 99.0\%$ ), Bismuth nitrate ( $\text{Bi}(\text{NO}_3)_3 \cdot 5\text{H}_2\text{O}$ , Sigma-Aldrich,  $\geq 98.0\%$ ), and Ferric nitrate ( $\text{Fe}(\text{NO}_3)_3 \cdot 9\text{H}_2\text{O}$ , Sigma-Aldrich,  $\geq 98.0\%$ ) as starting materials were used to prepare  $\text{La}_{1-x}\text{Bi}_x\text{FeO}_3$  ( $x = 0, 0.2, 0.4, 0.6,$  and  $0.8$ ). The raw materials were dissolved in 100 mL of bi-distilled water to form a clear solution and then evaporated at  $60^\circ\text{C}$  with continuous stirring using a magnetic stirrer. Additionally, nitric acid was added drop wise during the stirring process to control the pH. On the other hand, Citric acid, Sigma-Aldrich,  $\geq 98.0\%$  as a fueling agent, Ethylene Diamine Tetra Acetic acid (EDTA, Sigma-Aldrich,  $\geq 98.0\%$ ), as a chelating agent, and Ethylene glycol, Sigma-Aldrich,  $\geq 98.0\%$ , as a polymerization agent were added to the solution and forming brown precursor solution. In the next step, the solution is heated to  $120^\circ\text{C}$  ( $10^\circ\text{C} \cdot \text{min}^{-1}$ ) until it becomes a dry gel. After that, the temperature increases to  $350^\circ\text{C}$ , and the gel turns into a puff. The obtained puff was dried at  $110^\circ\text{C}$  for 10 h to become a dark brown powder, and the soft powders were calcined at  $600^\circ\text{C}$  for 12 h with ( $5^\circ\text{C} \cdot \text{min}^{-1}$ ). Finally, the light brown powder was heated in the air using a tubular furnace (R 50/500/13 Nabertherm model) at  $800^\circ\text{C}$  for 24 h. This operation is repeated two times to obtain the phase. Nanocrystalline Yam orange powders of  $\text{La}_{1-x}\text{Bi}_x\text{FeO}_3$  ( $x = 0, 0.2, 0.4, 0.6$  and  $0.8$ ) were labeled LBF0, LBF2, LBF4, LBF6 and LBF8, respectively. The described reactions are shown in Equation (1):



Phase identification and unit cell parameter determination were checked using powder X-ray diffraction (XRD) at room temperature. Powder X-ray diffraction data were recorded using a Proto AXRD

Benchtop diffractometer (Bragg-Brentano configuration), in the  $2\theta$  range of  $10^\circ$  to  $80^\circ$ , with  $\text{CuK}\alpha$  radiation ( $\lambda=1.5418 \text{ \AA}$ ). The tube voltage and tube current are 30 kV and 20 mA, respectively. The crystallite sizes of the synthesized powders were determined from the full width at half-maximum (FWHM) in radians using the Scherrer formula [30] as shown in Equation (2):

$$D = \frac{k \cdot \lambda}{\beta_{\text{hkl}} \cos \theta} \quad (2)$$

where  $k$  is the shape function for which a value of 0.9 is used,  $\lambda$  is the wavelength of the incident X-Ray ( $\text{Cu-K}\alpha=1.5418 \text{ \AA}$ ),  $\theta$  is the diffraction angle, and  $\beta_{\text{hkl}}$  is full-width at half-maximum (FWHM) of the XRD peaks.  $\beta_{\text{hkl}}$  is appreciated as the estimated correct broadening of the sample. The morphology of the synthesized samples was examined using the scanning electron microscope model Thermo Scientific Quattro ESEM. At the same time, their compositions were analyzed by Energy dispersive X-ray (EDX) spectroscopy using a Zeiss SmartEDX detector integrated into Zeiss Evo15 Scanning Electron Microscope (SEM), intended to observe dry and conducting samples. The Fourier transform infrared (FTIR) spectra were recorded in the range  $4000 \text{ cm}^{-1}$  to  $450 \text{ cm}^{-1}$  using IR Spirit - Shimadzu Fourier transform infrared (FTIR) spectrometer. The as-synthesized powders were measured using a Shimadzu -1900 UV visible spectrometer.

## 3. Results and discussion

X-Ray Powder Diffraction patterns of the parent and substituted compounds are shown in Figure 1.

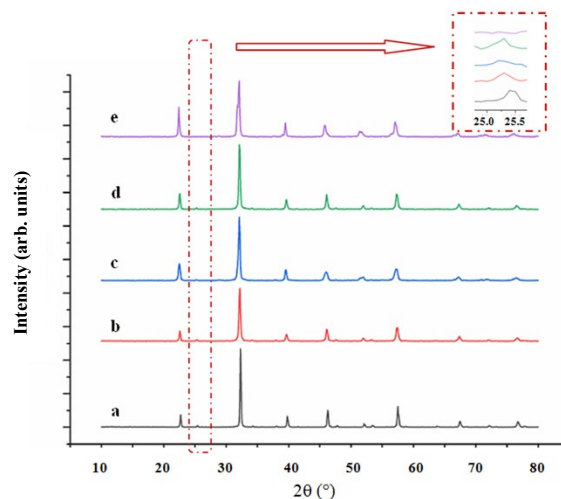


**Figure 1.** X-ray powder diffraction pattern of  $\text{La}_{1-x}\text{Bi}_x\text{FeO}_3$  (a)  $x=0$ , (b)  $x=0.2$ , (c)  $x=0.4$ , (d)  $x=0.6$ , and (e)  $x=0.8$ .

**Table 1.** Crystallographic parameters obtained by the rietveld refinement of  $\text{La}_{1-x}\text{Bi}_x\text{FeO}_3$  samples.

Sample	Space group	Lattice parameters ( $\text{\AA}$ )			Volume ( $\text{\AA}^3$ )	$\chi^2$
		a	b	c		
LBF0	Pbnm	5.5542	5.5667	7.8534	242.82	1.16
LBF2	Pbnm	5.5499	5.5660	7.8525	242.57	1.21
LBF4	Pbnm	5.5491	5.5874	7.8282	242.71	1.52
LBF6	Pbnm	5.5553	5.5641	7.8565	242.85	1.23
LBF8	R3c	5.5695	5.5695	13.8081	428.32	1.46

Structural analysis has been performed by Rietveld refinement method [31], using the MAUD 2.33 software [32]. All peaks of La<sub>1-x</sub>Bi<sub>x</sub>FeO<sub>3</sub> (x = 0, 0.2, 0.4, 0.6) samples can be refined on the orthorhombic Pbnm (N° 62) space group. However, the XRD pattern collected from the La<sub>0.2</sub>Bi<sub>0.8</sub>FeO<sub>3</sub> sample exhibited notable features such as an increased intensity of the first peak located at 22.40°, the disappearance of the peak located at 25.30° and the splitting of the peak at 32.1°, indicating a transition to the rhombohedral R3c (N° 161) space group. Bi-doping inevitably induces a transition in perovskite materials from Pbnm to R3c structure, given that LaFeO<sub>3</sub> has an orthorhombic Pbnm structure, while BiFeO<sub>3</sub> has a rhombohedral R3c structure. The refinement results are summarized in Table 1, and the final Rietveld refinement plot is presented in Figure 2.

The fitting quality is assessed from the estimated goodness of fit  $\chi^2$  factor (see Eqts. N° 3, 4 and 5), which is defined as:

$$\chi^2(\text{goodness of fit}) = \left( \frac{R_{wp}}{R_{exp}} \right)^2 \quad (3)$$

where

$$R_{wp}(\text{weighted profile R factor}) = \left[ \frac{\sum_i w_i [y_i(\text{obs}) - y_i(\text{calc})]^2}{\sum_i w_i [y_i(\text{obs})]^2} \right]^{1/2} \quad (4)$$

and

$$R_{exp}(\text{expected R factor}) = \left[ \frac{(N-P)}{\sum_i^N w_i y_i(\text{obs})^2} \right]^{1/2} \quad (5)$$

Here,  $Y_i$ ,  $Y_{ci}$  is the respective experimental and calculated intensity value,  $w_i$  is the variance,  $N$  is the number of points,  $P$  is the number of refined parameters,  $(N-P)$  is the degree of freedom. It is important to note that the best fits are those where  $\chi^2 < 2$  [33-35].

No apparent second phase can be detected in the doped samples, indicating complete dissolution of Bi<sup>3+</sup> ions in the host lattice by substituting the La<sup>3+</sup>. The unit cell volume of La<sub>1-x</sub>Bi<sub>x</sub>FeO<sub>3</sub>, where  $x$  in the range [0, 0.6], remains constant within the error standard deviation (e.s.d.) with the added amount of Bi. This constancy is attributed to the very close radius of Bi<sup>3+</sup> ion ( $r(\text{Bi}^{3+}) = 1.17\text{\AA}$ ) compared to the La<sup>3+</sup> ion ( $r(\text{La}^{3+}) = 1.16\text{\AA}$ ) [36], evident from the slight shift of the XRD peak towards a higher  $2\theta$  value, as shown in Figure 2. Calculated lattice parameters and unit cell volume of the La<sub>1-x</sub>Bi<sub>x</sub>FeO<sub>3</sub> samples are listed in Table 2. Crystallites are predominantly oriented along the (112) plane in the orthorhombic structures and the (110) plane in the hexagonal ones.

We know that the breadth of the Bragg peak is a combination of both instrument and sample-dependent effects [37]. So, we use the LaB<sub>6</sub> standard for instrumental broadening correction. The corrected

broadening corresponding to the diffraction peaks of La<sub>1-x</sub>Bi<sub>x</sub>FeO<sub>3</sub> was estimated by using the following Equation (6) [38,39]:

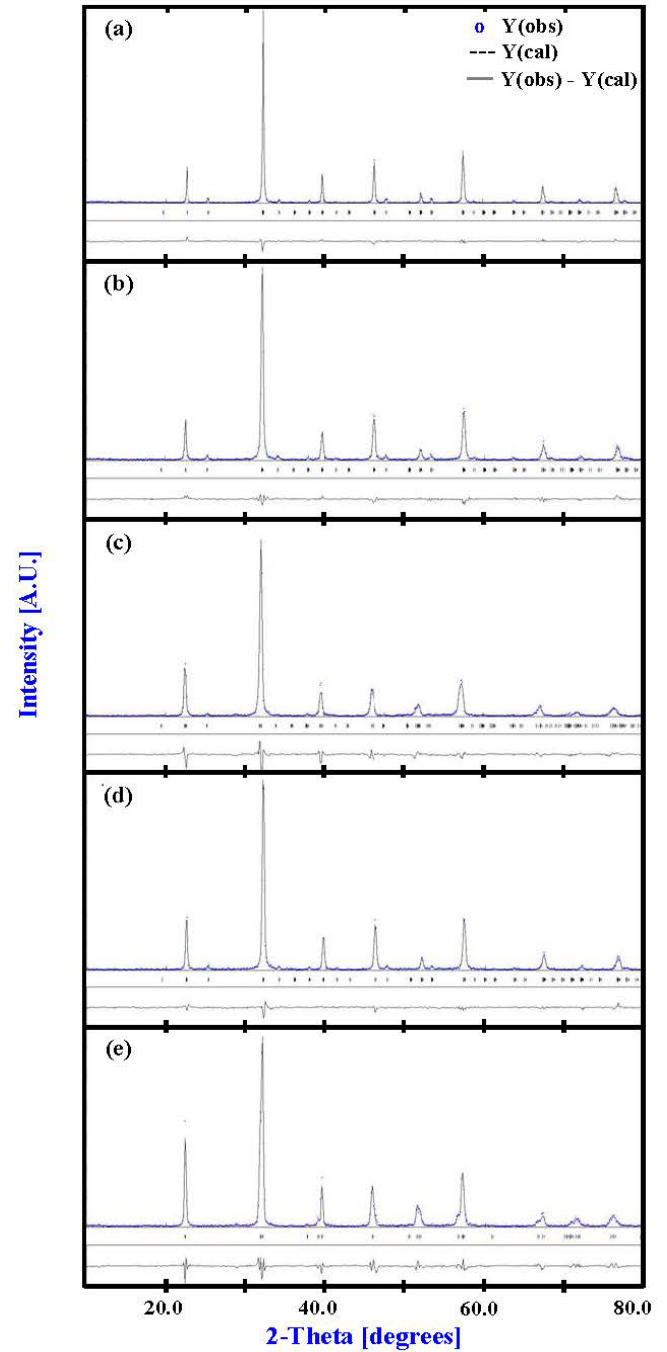


**Figure 2.** Rietveld refinement of experimental XRD pattern of La<sub>1-x</sub>Bi<sub>x</sub>FeO<sub>3</sub> samples (a) x=0, (b) x=0.2, (c) x=0.4, (d) x=0.6 and (e) x=0.8 refined at room temperature.

**Table 2.** Crystallites sizes D for highest intense peak of La<sub>1-x</sub>Bi<sub>x</sub>FeO<sub>3</sub> samples.

Samples	(hkl)	2θ (°)	FWHM=β (°)	Crystallites size (nm)
LBF0	(112) <sub>o</sub>	32.2134	0.1650	50
LBF2	(112) <sub>o</sub>	32.1828	0.2761	30
LBF4	(112) <sub>o</sub>	32.1426	0.2604	32
LBF6	(112) <sub>o</sub>	32.1027	0.2819	30
LBF8	(110) <sub>R</sub>	31.9341	0.4323	19

O: Orthorhombic; R: Rhombohedral

$$\beta_{hkl} = (\beta_{measured}^2 - \beta_{instrument}^2)^{1/2} \quad (6)$$

The crystallite sizes of the (112) characteristic peak for orthorhombic phases and the (110) distinct peak for rhombohedral phase obtained from X-ray analysis are presented in Table 2. It can be observed that the crystallite sizes (D) of the orthorhombic Bi-substituted LaFeO<sub>3</sub> samples (i.e. LBF2, LBF4 and LBF6) extracted from some reflections remained almost constant at about 30 nm, decreasing to 19 nm for LBF8.

A quantitative analysis of pure and Bi<sup>3+</sup>-substituted LaFeO<sub>3</sub> nanoparticles was determined using energy dispersive X-ray (EDX) spectroscopy by performing spot measurements on powder samples. The EDX analysis indicates consistency with the expected stoichiometry within the limit of experimental error. The EDX spectrum confirms the formation of the desired compounds (Figure 3).

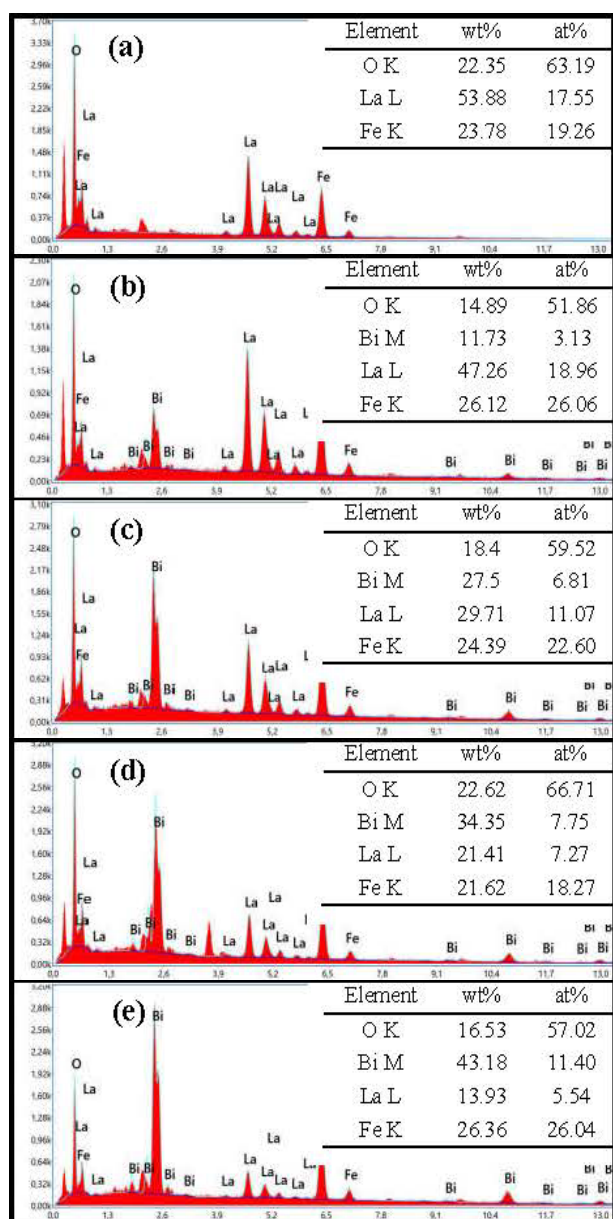


Figure 3. EDX spectra with percentage of elements for La<sub>1-x</sub>Bi<sub>x</sub>FeO<sub>3</sub> samples (a) x=0, (b) x=0.2, (c) x=0.4, (d) x=0.6, and (e) x=0.8.

Scanning electron microscopy (SEM) was used to observe the surface morphology of the prepared samples. Figure 4 shows that the dispersion and morphology have not changed significantly despite the doping samples with Bi<sup>3+</sup> ions. However, with an increase in the concentration of Bi substitution, aggregates form and become bigger.

Figure 5 shows the FTIR spectra of pure and Bi-substituted LaFeO<sub>3</sub> in the range 4000 cm<sup>-1</sup> to 450 cm<sup>-1</sup>. It is noteworthy that the respective ratio spectra are almost similar, differing mainly in peak intensity, attributed to variations in molar concentration composition. The bands between 700 cm<sup>-1</sup> and 400 cm<sup>-1</sup> were mainly attributed to the formation of metal oxides, while the strong absorption band at about 536 cm<sup>-1</sup> can be attributed to the (Fe-O) bending vibration being characteristics of the octahedral FeO<sub>6</sub> groups in La<sub>1-x</sub>Bi<sub>x</sub>FeO<sub>3</sub> [40]. On the other hand, the bands at 717 cm<sup>-1</sup> might be attributed to the bending vibration of the La-O bonds [41]. Furthermore, two close bands are observed: the first at 1385 cm<sup>-1</sup>, attributed to NO<sub>3</sub><sup>-</sup>, whereas the second at 1485 cm<sup>-1</sup>, attributed to N-H. Both bands originate from reacted precursor raw materials; they are closely located and exhibit weak intensity [42].

The La/Fe-O bending vibration modes do not shift toward a higher or lower frequency with increasing Bi content up to x=0.6, which confirms no deformation of the lattice and, thus, no changes in the La/Fe-O bond length, supported by the XRD analysis.

UV-Visible spectroscopy is employed to characterize the optical properties of the LBF nanoparticles. The band gaps of the prepared samples were extracted from Tauc's plot. The relation between absorption coefficient ( $\alpha$ ) and incident photon energy ( $h\nu$ ) can be determined using Tauc's equation, as shown in Equation (7) [43]:

$$(ah\nu)^2 = A(h\nu - E_g) \quad (7)$$

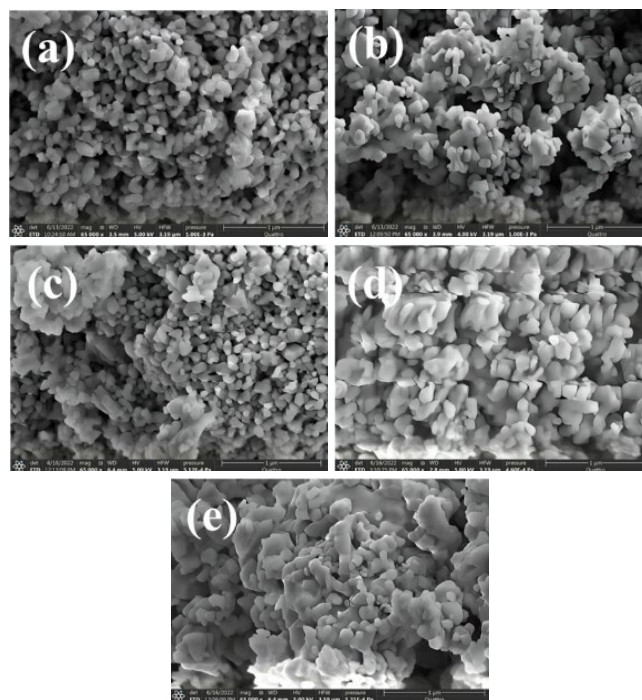
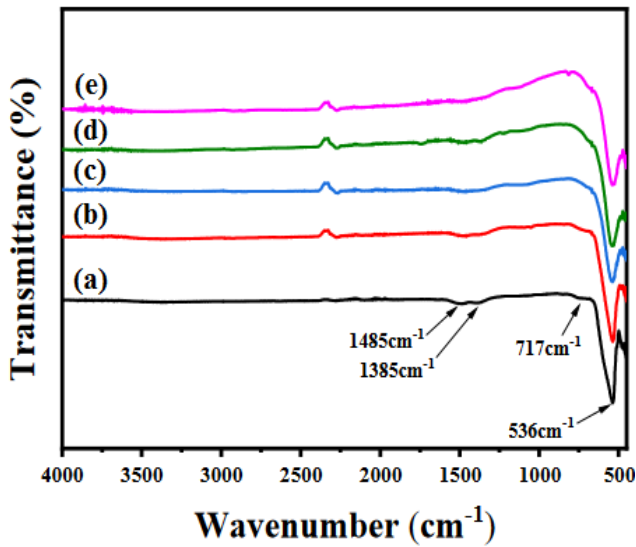


Figure 4. SEM micrographs of La<sub>1-x</sub>Bi<sub>x</sub>FeO<sub>3</sub> samples (a) x=0, (b) x=0.2, (c) x=0.4, (d) x=0.6, and (e) x=0.8.



**Figure 5.** FTIR spectra of La<sub>1-x</sub>Bi<sub>x</sub>FeO<sub>3</sub> nanoparticles (a) x=0, (b) x=0.2, (c) x=0.4, (d) x=0.6, and (e) x=0.8.

where  $\alpha$  is the optical absorption coefficient,  $h\nu$  is the photon energy,  $E_g$  is the direct band gap, and  $A$  is constant. The extrapolation of the linear parts of the curves toward absorption equal to zero gives  $E_g$  for direct transitions (Figure 6). The estimated direct band gaps of pure LaFeO<sub>3</sub> is 2.2 eV. However, these values decrease to 1.86 eV, 1.76 eV, 1.54 eV and 1.35 eV for Bi substitutions of 20%, 40%, 60% and 80% respectively (Table 3).

The presented data unequivocally indicates that all La<sub>1-x</sub>Bi<sub>x</sub>FeO<sub>3</sub> samples ( $x=0.0, 0.2, 0.4, 0.6,$  and  $0.8$ ) exhibit an energy gap ( $E_g$ ) falling within the range of 1.35 eV to 2.2 eV, classifying them as semiconductor materials [44].

The  $E_g$  decreases continuously as the substitution of Bi increases up to 80% (Figure 7). The Fe–O octahedral restructuring of molecular orbitals and the length scale of nanoparticles can also reduce the value of  $E_g$  [45–47]. It may also be due to the direct energy transfer between the semiconductor-excited states and the 3d levels of Bi<sup>3+</sup> ions [48]. Moreover, the very low band gap value of La<sub>0.2</sub>Bi<sub>0.8</sub>FeO<sub>3</sub> is interesting for application in photocatalytic [49] and can make its structure promising for solar cell applications.

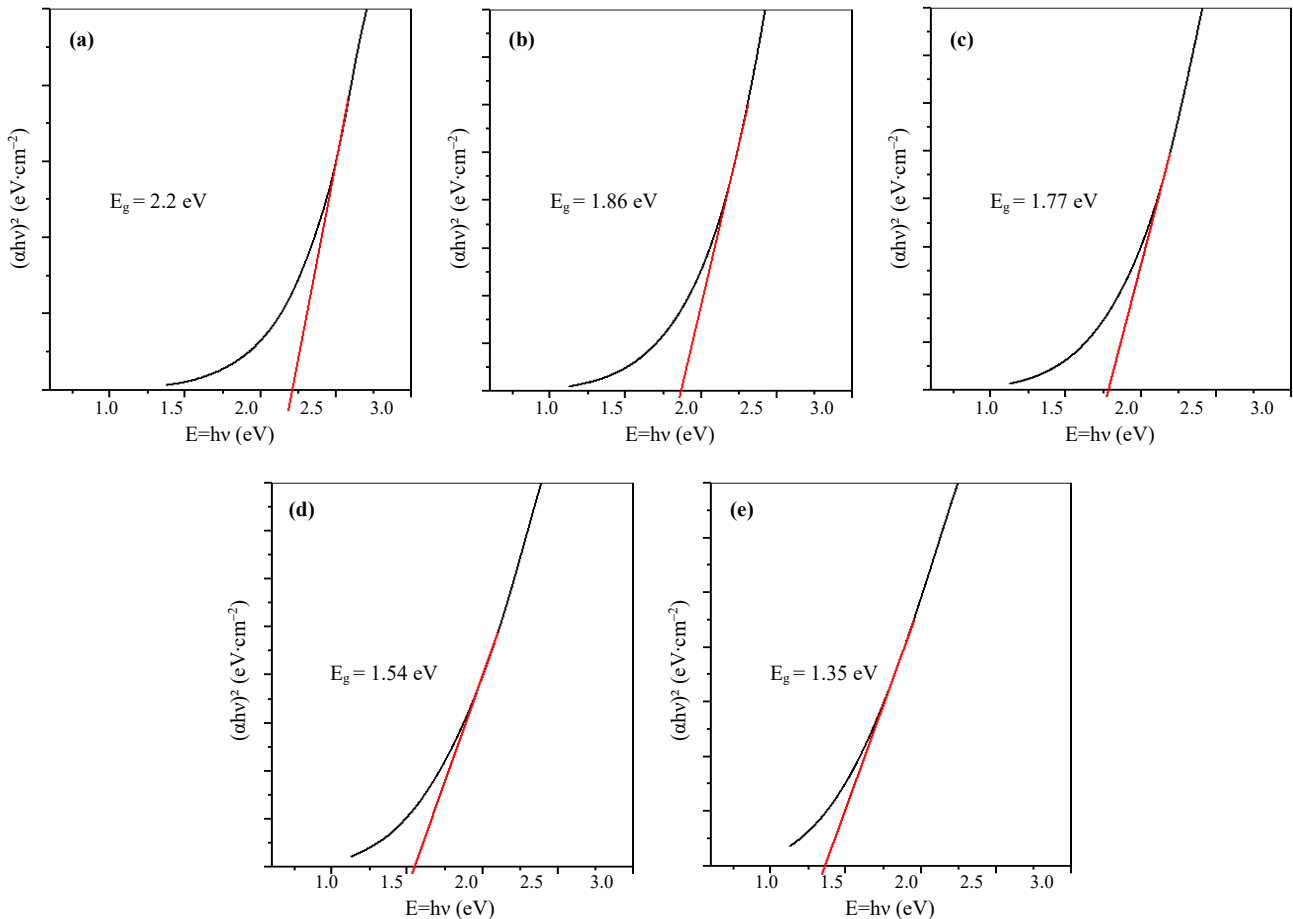


**Figure 6.** Plot of  $(\alpha h\nu)^2$  versus  $h\nu$  for La<sub>1-x</sub>Bi<sub>x</sub>FeO<sub>3</sub> samples (a) x=0, (b) x=0.2, (c) x=0.4, (d) x=0.6, and (e) x=0.8.

**Table 3.** Optical band gap energy of La<sub>1-x</sub>Bi<sub>x</sub>FeO<sub>3</sub> ( $x = 0.0, 0.2, 0.4, 0.6, 0.8$ ) nanoparticles.

Sample	LBF0	LBF2	LBF4	LBF6	LBF8
$E_g$ (eV)	2.2	1.85	1.76	1.54	1.35

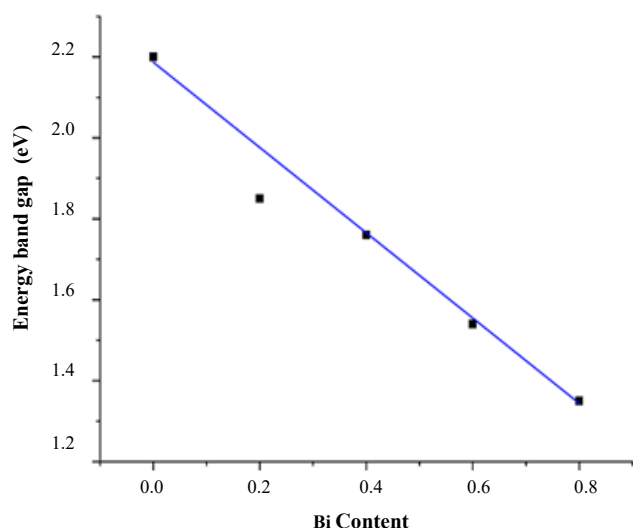


Figure 7. Band gap energy vs. Bi substituted content of LaFeO<sub>3</sub> samples.

#### 4. Conclusions

Nanoparticles of La<sub>1-x</sub>Bi<sub>x</sub>FeO<sub>3</sub> ( $x = 0, 0.2, 0.4, 0.6, 0.8$ ) have been prepared by the sol-gel self-ignition method. XRD patterns indicate that Bi ions incorporate into La sites in the crystals without changing the orthorhombic structure from  $x=0$  up to  $x=0.6$ , while the phase changes its structure to hexagonal at  $x=0.8$ . The unit cell volume of the La<sub>1-x</sub>Bi<sub>x</sub>FeO<sub>3</sub> orthorhombic structure remains constant within the range of the error standard deviation (e.s.d.) with increasing Bi concentration. This result is due to the very close radius of the Bi<sup>3+</sup> ion ( $r(\text{Bi}^{3+}) = 1.17\text{\AA}$ ) compared to the La<sup>3+</sup> ion ( $r(\text{La}^{3+}) = 1.16\text{\AA}$ ). The crystallite sizes ( $D$ ) vary between 19 nm and 50 nm, remaining almost constant at about 30 nm for the orthorhombic Bi-substituted LaFeO<sub>3</sub> samples ( $x = 0.2, 0.4, 0.6$ ). No secondary phases were observed in both pure and Bi-substituted samples, indicating the homogenous substitution of Bi ions into the LaFeO<sub>3</sub> lattice structure. EDX analysis confirmed the quantitative incorporation of Bismuth into the host lattice. SEM micrographs revealed that the morphology of the pure LaFeO<sub>3</sub> consists loosely dispersed clusters of tiny particles, whereas the Bi-substituted material displayed larger aggregates breaking up into small clusters with increased Bi concentration. FTIR analysis confirms the formation of LaFeO<sub>3</sub> and Bi-substituted LaFeO<sub>3</sub> samples. The band gap energy ( $E_g$ ) values decrease from 2.2 to 1.85, 1.76, 1.44, and 1.35 eV, with increasing Bi-substituted from 0% to 20%, 40%, 60%, and 80% respectively. This decrease may be attributed to the direct energy transfer between the semiconductor-excited states and the 3d levels of Bi<sup>3+</sup> ions. These findings suggest La<sub>0.8</sub>Bi<sub>0.2</sub>FeO<sub>3</sub> as a competitive candidate for use as an electron transport material in inorganic perovskite solar cells.

#### Acknowledgment

The authors gratefully acknowledge the financial support of Directorate General for Scientific Research and Technological Development–DGRSDT–(PRFU Project N°. B00L02UN390120180003), Ministry of Higher Education and Scientific Research – ALGERIA.

#### References

- [1] L. J. Berchmans, V. Leena, K. Amalajyothi, S. Angappan, and A. Visuvasam, "Preparation of lanthanum ferrite substituted with Mg and Ca," *Materials and Manufacturing Processes.*, vol. 24, no. 5, pp. 546-549, 2009.
- [2] N. Q. Minh, "Ceramic Fuel Cells," *Journal of the American Ceramic Society*, vol. 76, pp. 563-588, 1993.
- [3] A. Delmaster, D. Mazza, S. Ronchetti, M. Vallino, R. Spinicci, P. Brovotto, and M. Salis, "Synthesis and characterization of non-stoichiometric LaFeO<sub>3</sub> perovskite," *Materials Science Engineering: B*, vol. 79, pp. 140-145, 2001.
- [4] S. L. Bai, X. X. Fu, J. Z. Wang, Q. H. Yang, Y. H. Sun, and S. L. Zeng, "Photocatalysis of LaFeO<sub>3</sub> (in Chinese)," *Chinese Journal of Applied Chemistry*, vol. 17, no. 3, pp. 343-345, 2000.
- [5] P. Song, Q. Wang, Z. Zhang, and Z. Yang, "Synthesis and gas sensing properties of biomorphic LaFeO<sub>3</sub> hollow fibers templated from cotton," *Sensors and Actuators B: Chemical*, vol. 147, no. 1, pp. 248-254, 2010.
- [6] Y. Shimizu, M. Shimabukuro, H. Arai, and T. Seiyama, "Enhancement of humidity sensitivity for perovskite-type oxides having semiconductivity," *Chemistry Letters*, vol. 14, no. 7, pp. 917-920, 1985.
- [7] G. Martinelli, M. C. Carotta, M. Ferrini, Y. Sadaoka, and E. Traversa, "Screen-printed perovskite-type thick films as gas sensors for environmental monitoring," *Sensors and Actuators B: Chemical*, vol. 55, no. 2-3, pp. 99-110, 1999.
- [8] P. Wang, Y. He, Y. Mi, J. Zhu, F. Zhang, Y. Liu, Y. Yang, M. Chen, and D. Cao, "Enhanced photoelectrochemical performance of LaFeO<sub>3</sub> photocathode with Au buffer layer," *RSC Advances*, vol. 9, no. 46, pp. 26780-26786, 2019.
- [9] M. Khairy, A. H. Mahmoud, and K. M. S. Khalil, "Synthesis of highly crystalline LaFeO<sub>3</sub> nanospheres for phenoxazinone synthase mimicking activity," *RSC Advances*, vol. 11, pp. 17746-17754, 2021.
- [10] Q. Peng, J. Wang, Y. W. Wen, B. Shan, and R. Chen, "Surface modification of LaFeO<sub>3</sub> by Co-Pi electrochemical deposition as an efficient photoanode under visible light," *RSC Advances*, vol. 6, pp. 26192-26198, 2016.
- [11] X. T. Yin, H. Huang, J-Li. Xie, D. Dastan, J. Li, Y. Liu, X-M. Tan, X-C. Gao, W. A. Shah, and X. G. Ma, "High-performance visible-light active Sr-doped porous LaFeO<sub>3</sub> semiconductor prepared via sol-gel method," *Green Chemistry Letters and Reviews*, vol. 15, no. 3, pp. 546-556, 2022.
- [12] S. D. Khairnar, and V. S. Shrivastava, "Facile synthesis of nickel oxide nanoparticles for the degradation of methylene blue and rhodamine B dye: A comparative study," *Journal of Taibah University for Science*, vol. 13, pp. 1108-1118, 2019.
- [13] V. A. Adole, T. B. Pawar, P. B. Koli, and B. S. Jagdale, "Exploration of catalytic performance of nano-La<sub>2</sub>O<sub>3</sub> as an efficient catalyst for dihydropyrimidinone/thione synthesis and gas sensing," *Journal of Nanostructure in Chemistry*, vol. 9, pp. 61-76, 2019.
- [14] I. M. Peters, and T. Buonassisi, "Energy yield limits for single-junction solar cells," *Joule*, vol. 2, no. 6, pp. 1160-1170, 2018.

- [15] F. Moradi, Z. Shariatinia, N. Safari, and E. Mohajerani, "Boosted performances of mesoscopic perovskite solar cells using LaFeO<sub>3</sub> inorganic perovskite nanomaterial," *Journal of Electroanalytical Chemistry*, vol. 916, p. 116376, 2022.
- [16] L. John Berchmans, R. Sindhu, S. Angappan, and C. O. Augustin, "Effect of antimony substitution on structural and electrical properties of LaFeO<sub>3</sub>," *Journal of Materials Processing Technology*, vol. 207, no. 1-3, pp. 301-306, 2008.
- [17] Q. Guo, X. Li, H. Wei, Y. Liu, L. Li, X. Yang, X. Zhang, H. Liu, and Z. Lu, "Sr, Fe Co-doped perovskite oxides with high performance for oxygen evolution reaction," *Frontiers in Chemistry*, vol. 7, p. 224, 2019.
- [18] B. Irshad, H. Shahid, K. Wasi, and S. I. Patil, "Effect of Zn doping on structural, magnetic and dielectric properties of LaFeO<sub>3</sub> synthesized through sol-gel auto-combustion process," *Materials Research Bulletin*, vol. 48, no. 11, pp. 4506-4512, 2013.
- [19] S. Manzoor, and S. Husain, "Influence of Zn doping on structural, optical and dielectric properties of LaFeO<sub>3</sub>," *Materials Research Express*, vol. 5, no. 5, p. 055009, 2018.
- [20] I. N. Sora, F. Fontana, R. Passalacqua, C. Ampelli, S. Perathoner, G. Centi, F. Parrino, and L. Palmisano, "Photoelectrochemical properties of doped lanthanum orthoferrites," *Electrochimica Acta*, vol. 109, pp. 710-715, 2013.
- [21] Y. Fang, L. Mei, Y. Hu, L. Jinpei, H. Kangling, H. Yun, and L. Qing, "Magnetic and dielectric properties of Ca<sup>2+</sup> doped Bi<sub>0.9</sub>La<sub>0.1</sub>FeO<sub>3</sub> nanoparticles prepared by the sol-gel method," *Indian Journal of Engineering and Materials Sciences*, vol. 26, no. 1, pp. 36-42, 2019.
- [22] M. I. Díez-García, and R. Gómez, "Metal doping to enhance the photoelectrochemical behavior of LaFeO<sub>3</sub> photocathodes," *ChemSusChem*, vol. 10, no. 11, pp. 2457-2463, 2017.
- [23] L. Qingsheng, Z. You, S. J. Zeng, and H. Guo, "Infrared properties of Mg-doped LaFeO<sub>3</sub> prepared by sol-gel method," *Journal of Sol-Gel Science and Technology*, vol. 80, pp. 860-866, 2016.
- [24] X. Liu, B. Cheng, J. Hu, H. Qin, and M. Jiang, "Preparation, structure, resistance and methane-gas sensing properties of nominal La<sub>1-x</sub>Mg<sub>x</sub>FeO<sub>3</sub>," *Sensors and Actuators B: Chemical*, vol. 133, pp. 340-344, 2008.
- [25] D. Triyono, U. Hanifah, and H. Laysandra, "Structural and optical properties of Mg-substituted LaFeO<sub>3</sub> nanoparticles prepared by a sol-gel method," *Results in Physics*, vol. 16, p. 102995, 2020.
- [26] S. N. Fitria, and D. Triyono, "Structural analysis and dielectric properties of La<sub>1-x</sub>Bi<sub>x</sub>FeO<sub>3</sub> perovskite materials at room temperature," *Journal of Physics: Conference Series*, vol. 1153, p. 012071, 2019.
- [27] Q. Yao, C. Tian, Z. Lua, J. Wang, H. Zhou, and G. Rao, "Anti-ferromagnetic-ferromagnetic transition in Bi-doped LaFeO<sub>3</sub> nanocrystalline ceramics," *Ceramics International*, vol. 46, pp. 20472-20476, 2020.
- [28] L. Wanjun, Y. Fujun, X. Peng, J. Yunjie, L. Jiawei, Y. Xinsui, C. Xiaoqin, "Effect of Bi-doping on the electrocatalytic properties of LaFeO<sub>3</sub> powders prepared by sol-gel method", *Journal of Materials Science*, vol. 54, no. 10, pp.7460-7468, 2019.
- [29] M. A. Ahmed, A. A. Azab, and E. H. El-Khawass, "Structural, magnetic and electrical properties of Bi doped LaFeO<sub>3</sub> nano-crystals, synthesized by auto-combustion method," *Journal of Materials Science: Materials in Electronics*, vol. 26, pp. 8765-8773, 2015.
- [30] B. D. Cullity, *Elements of X-ray Diffraction*, 2nd ed., Massachusetts: Addison-Wesley Publishing Company, Inc., 1978.
- [31] G. Will, *Powder Diffraction: The Rietveld Method and the Two Stage Method to Determine and Refine Crystal Structures from Powder Diffraction Data*, Berlin Heidelberg: Springer-Verlag, 2006.
- [32] L. Lutterotti, "Total pattern fitting for the combined size-strain-stress-texture determination in thin film diffraction," *Nuclear Instruments and Methods B*, vol. 268, pp. 334-340, 2010.
- [33] B. H. Toby, "R factors in Rietveld analysis: How good is good enough?," *Powder Diffraction*, vol. 21, no. 1, pp. 67-70, 2006.
- [34] R. A. Young, *The Rietveld Method*; R. A., Young, Ed.; Oxford University Press, New York (US), pp. 1- 38, 1993.
- [35] J. Shah, A. Shukla, M. Kar, G. Gupta, S. Jain, and R. K. Kotnala, "ZnO nanoflakes self-assembled from the water splitting process using a hydroelectric cell," *Reaction Chemistry & Engineering*, vol. 7, no. 8, pp. 1836-1846, 2022.
- [36] R. D. Shannon, "Revised effective ionic radii and systematic studies of interatomic distances in halides and chalcogenides," *Acta Crystallographica Section A*, vol. 32, pp. 751-767, 1976.
- [37] P. Bindu, and S. Thomas, " Estimation of lattice strain in ZnO nanoparticles: X-ray peak profile analysis," *Journal of Theoretical and Applied Physics*, vol. 8, pp. 123-124, 2014.
- [38] V. Biju, S. Neena, V. Vrinda, and S. L. Salini, " Estimation of lattice strain in nanocrystalline silver from X-ray diffraction line broadening," *Journal of Materials Science*, vol. 43, pp. 1175-1179, 2008.
- [39] T. R. Jeena, A. M. E. Raj, and M. Bououdina, "Synthesis and photoluminescent characteristics of Dy<sup>3+</sup> doped Gd<sub>2</sub>O<sub>3</sub> phosphors," *Materials Research Express*, vol. 4, p. 025019, 2017.
- [40] M. Čebela, B. Jankovic, R. Hercigonja, M. J. Lukic, Z. Dohcevic-Mitrovic, D. Milivojevic, and B. Matovic, "Comprehensive characterization of BiFeO<sub>3</sub> powder synthesized by the hydrothermal procedure," *Processing and Application of Ceramics*, vol. 10, no. 4, pp. 201-208, 2016.
- [41] M. Ismael, and M. Wark, "Perovskite-type LaFeO<sub>3</sub>: Photoelectrochemical properties and photocatalytic degradation of organic pollutants under visible light irradiation," *Catalysts*, vol. 9, no. 4, p. 342, 2019.
- [42] P. Desai, and A. Athawale, "Microwave combustion synthesis of silver doped lanthanum ferrite magnetic nanoparticles", *Defence Science Journal*, vol. 63, no. 3, pp. 285-291, 2013.
- [43] J. I. Pankove, *Optical Processes in Semiconductors*, New Jersey: Prentice-Hall, Englewood Cliffs, 1971.
- [44] A. Yoshikawa, H. Matsunami, and Y. Nanishi, "Development and applications of wide bandgap semiconductors," in *Wide Bandgap Semiconductors*, K. Takahashi, A. Yoshikawa, and A. Sandhu, Eds. Berlin, Heidelberg: Springer Berlin Heidelberg, pp. 1-24, 2007.
- [45] M. Sivakumar, A. Gedanken, W. Zhong, Y. H. Jiang, Y. W. Du, I. Brukental, D. Bhattacharya, Y. Yeshurun, and I. Nowik, "Sonochemical synthesis of nanocrystalline LaFeO<sub>3</sub>", *Journal of Materials Chemistry*, vol. 14, pp. 764-769, 2004.

- [46] M. Popa, J. Frantti, and M. Kakihana, "Lanthanum ferrite  $\text{LaFeO}_3$  doped nanopowders obtained by the polymerizable complex method", *Solid State Ionics*, vol. 154, pp. 437-445, 2002.
- [47] M. A. Matin, M. N. Hossain, M. M. Rhaman, F. A. Mozahid, Md. S. Ali, M. Hakim, and M. F. Islam, "Dielectric and optical properties of Ni-doped  $\text{LaFeO}_3$  nanoparticles," *SN Applied Sciences*, vol. 1, p. 14792, 2019.
- [48] F. J. Brieler, M. Froba, L. Chen, P. J. Klar, W. Heimbrod, H-A. Krug von Nidda, A. Loidl, "Ordered arrays of II/VI diluted magnetic semiconductor quantum wires: Formation within mesoporous MCM-41 silica," *Chemistry European Journal*, vol. 8, no. 1, pp. 185-194, 2002.
- [49] R. Dhinesh Kumar, R. Thangappan, and R. Jayavel, "Synthesis and characterization of  $\text{LaFeO}_3/\text{TiO}_2$  nanocomposites for visible light photocatalytic activity," *Journal of Physics and Chemistry of Solids*, vol. 101, pp. 25-33, 2017.